LASER & PHOTONICS REVIEWS

www.lpr-journal.org

Low Threshold Room Temperature Polariton Lasing from Fluorene-Based Oligomers

Mengjie Wei, Arvydas Ruseckas, Van T. N. Mai, Atul Shukla, Ilene Allison, Shih-Chun Lo, Ebinazar B. Namdas,* Graham A. Turnbull,* and Ifor D. W. Samuel**

Organic semiconductors possessing tightly bound Frenkel excitons are known to be attractive candidates for demonstrating polariton lasing at room temperature. As polariton lasing can occur without inversion, it is a potential route to very low threshold coherent light sources. However, so far, the thresholds of organic polariton lasers have generally been much higher than those of organic photon lasers. Here this problem has been addressed by investigating two new organic molecules with a structure combining fluorene and carbazole groups. The materials are readily deposited from solution and exhibit high photoluminescence quantum yields, high absorption coefficients, and large radiative decay rates in neat films. Room temperature polariton lasing is realized in both materials with incident thresholds of 13.5 and 9.7 μJ cm^{-2}, corresponding to absorbed thresholds of 3.3 and 2.2 μJ cm^{-2}, respectively. These are the lowest values reported to date for polariton lasing in organic semiconductor materials, and approach typical values for organic photon lasers. The step-like power dependent blue-shift of polariton modes indicates an interplay between different depletion channels of the exciton reservoir. This work brings practical room temperature polaritonic devices and future realization of electrically driven polariton lasers a step closer.

1. Introduction

Exciton-polaritons are quasiparticles hybridizing light and matter.[1,2] They are formed in confined systems where the energy exchange rate between excitons and cavity photons is much faster than their respective decay rates.[3] In this case, a strong exciton–photon coupling regime is established wherein two new eigenstates, the lower polariton branch (LPB) and the upper polariton branch (UPB), inherit characteristics from both excitons and photons. By electrically or optically pumping the system, polaritons can scatter along the LPB, accumulate in the ground polariton state, and escape from the cavity through photon decay. Under suitable conditions, polaritons macroscopically occupy the ground state, via stimulated polariton scattering, leading to coherent light emission known as polariton lasing.[4] This process occurs without a requirement for population inversion, and the polariton lasing threshold may potentially be much lower than that of a conventional photon laser in the same cavity configuration. This has been observed experimentally in both inorganic and organic microcavities.[5–7]

Organic semiconductors are of particular interest for polariton lasing because they possess tightly bound Frenkel excitons with high oscillator strength, which enable stable exciton-polaritons at room temperature.[8] Room temperature polariton lasing in organic semiconductors has been successfully explored in several material systems, including single crystal,[9] oligomers,[10–13] polymers,[14,15] and fluorescent proteins.[7,16]

Further progress in reducing polariton lasing thresholds requires progress in materials. The material requirements for

Dr. M. Wei, Dr. A. Ruseckas, Prof. G. A. Turnbull, Prof. I. D. W. Samuel
Organic Semiconductor Center
SUPA
School of Physics and Astronomy
University of St Andrews
St Andrews KY16 9SS, UK
E-mail: gat@st-andrews.ac.uk; idws@st-andrews.ac.uk

Dr. V. T. N. Mai, A. Shukla, I. Allison, Prof. S.-C. Lo, Prof. E. B. Namdas
Center for Organic Photonics & Electronics
The University of Queensland
Brisbane QLD 4072, Australia
E-mail: s.lo@uq.edu.au e.namdas@uq.edu.au

Dr. V. T. N. Mai, I. Allison, Prof. S.-C. Lo
School of Chemistry and Molecular Biosciences
The University of Queensland
Brisbane QLD 4072, Australia

A. Shukla, Prof. E. B. Namdas
School of Mathematics and Physics
The University of Queensland
Brisbane QLD 4072 Australia

The ORCID identification number(s) for the author(s) of this article can be found under https://doi.org/10.1002/lpor.202100028

© 2021 The Authors. Laser & Photonics Reviews published by Wiley-VCH GmbH. This is an open access article under the terms of the Creative Commons Attribution License, which permits use, distribution and reproduction in any medium, provided the original work is properly cited.

DOI: 10.1002/lpor.202100028

polariton lasers differ from those for photon lasers because of the need for strong light–matter coupling. This means that strongly absorbing films are required which maintain reasonable photoluminescence quantum yields (PLQYs) at very high chromophore concentrations. So, whilst for photon lasers, dilution of a chromophore [e.g., 4-(dicyanomethylene)-2-methyl-6-(4-dimethylaminostyryl)-4*H*-pyran (DCM) in a host such as Alq_3] is a very effective approach to reducing threshold, it would lead to the loss of strong coupling and so is not a suitable approach for polariton lasing. High concentration of chromophores (or preferably neat films) is required to achieve large Rabi splitting for clear observation of strong light–matter coupling, especially for organic materials with broadened excitonic features. Organic materials for photon lasing normally have considerable Stokes shifts, where the overlap between the absorption and emission spectra is weak to minimize the absorption at lasing wavelength, while organic laser dyes for polariton lasing ideally should have relatively small Stokes shifts so that both absorption and emission fall in the region of high reflectivity of the dielectric mirrors typically used. To achieve efficient radiative pumping of the lower polariton states, a good overlap between the LPB and the emission spectrum is necessary.[17] Additionally, whilst there is no specific requirement on the linewidth of excitonic transitions of organic materials for photon lasing, the literature suggests that narrow linewidths such as that found in J-aggregates are needed for strong coupling and polariton lasing, although this is a matter of debate.[8]

Here we report a study of polariton lasing in two fluorene derivatives containing carbazole and dihexylfluorene units. The design strategy of introducing carbazole groups at two ends of the fluorene core was inspired by polyfluorene (PFO) and 4,4′-bis[(*N*-carbazole) styryl]biphenyl (BSB-Cz). PFO has been reported to have attractive properties of high PLQY, high radiative rate (10^9 s^{-1}), and uniform morphology of films processed from solution.[18] Polariton lasing in PFO was observed at a low threshold of 28 μJ cm^{-2} pumped by a femtosecond pulsed laser, despite the inhomogeneous broadened excitonic transition due to disordered chain segments, which proved fluorene-cored organic molecules are promising polariton lasing materials. However, the chain conformation of PFO can be highly sensitive to processing conditions, resulting in films with different optoelectronic properties.[19–21] BSB-Cz also has promising properties for strong coupling, including high PLQY and high absorption coefficient.[22–24] BSB-Cz is, however, not solution processable.[25] We found that by replacing the bis-stilbene core of BSB-Cz with dihexylfluorene units, the problem of poor solubility of BSB-Cz can be overcome, while keeping the potential to be efficient laser materials.[26,27] The combination of fluorene and carbazole units provides a rigid structure with high solubility in common solvents, relatively high PLQY and very high absorption coefficient, originating from the extended π-conjugation of the molecule.[26,27] Furthermore, using small molecules avoids issues of polydispersity that arise in polymers, and plays a key role in determining photophysical properties. These factors make fluorene-carbazole based molecules appealing materials for polariton lasing studies. It has been previously shown that the absorption coefficient and radiative rate are dependent on the number of fluorene units.[28] Therefore, BSFCz and BSTFCz with respectively one fluorene and three fluorene units, were investigated. Strong exciton–photon coupling was demonstrated in distributed Bragg reflector (DBR) cavities containing each material. By optically pumping the cavities, room temperature polariton lasing was observed at a record low excitation density.

2. Results and Discussion

Figure 1a shows the chemical structures of BSFCz and BSTFCz, with dihexylfluorene cores and carbazole end units. Because strong coupling needs a high concentration of chromophores, the photophysical properties of these two molecules were studied in neat films and are shown in Figure 1b. In order to optimize the film quality for subsequent mirror deposition, we spin-coated the films from chlorobenzene, instead of chloroform as was previously used to make photon lasers.[26,27] The absorption spectrum of BSFCz exhibits an excitonic peak at 390 nm with a shoulder around 413 nm with an overall full width at half maximum (FWHM) of 73 nm, while the emission shows intense excimer emission with two peaks at 467 and 493 nm. In comparison, BSTFCz with three dihexylfluorene units exhibits slightly blue-shifted absorption and emission spectra, consistent with its larger energy gap between the highest occupied molecular orbital and the lowest unoccupied molecular orbital. This can be attributed to less planar links (with a dihedral angle of 40°) between the fluorenyl moieties than those in BSFCz[26] that partially disrupt the effective π-conjugation[27] in BSFCz. The more 3D structure in BSTFCz (as more dihexyl groups attached to the fluorene backbone) also reduces chromophore–chromophore intermolecular interaction in neat films (and hence gives a reduced red-shift when moving from solution to solid state).[29] The main absorption peak is at 387 nm with a FWHM of 68 nm, while the photoluminescence (PL) spectrum has a peak at 457 nm with partially resolved vibronic replicas at 439 and 485 nm. The neat films also exhibit relatively high PLQYs of around 30% for BSFCz and 32% for BSTFCz, high peak absorption coefficients of 2×10^5 cm^{-1}, very short fluorescence lifetime of several hundred picoseconds and high radiative rates ($\approx 10^9$ s^{-1}). It is worthwhile noting that the PLQY of BSTFCz in neat films is close to the lower boundary of the values reported in ref.[27] and the emission peak of 0–0 is weaker, which may be attributed to different processing conditions (spin coating from chlorobenzene instead of chloroform, leading to higher intermolecular interaction) used. To gain insight into the molecular orientation in thin films of BSFCz and BSTFCz, the optical constants were measured by ellipsometry (detailed in Section S2 in the Supporting Information). We interpret that BSTFCz molecules tend to align in the film plane, while BSFCz molecules have more isotropic packing.

We fabricated planar microcavities consisting of spin-coated neat films sandwiched in between DBR mirrors, as shown in Figure 1c. The DBRs were composed of pairs of Ta_2O_5/SiO_2 and their stopband was designed to cover most of the emission band and part of the absorption band at normal incidence. The solution-processed active layers were located at the centers of the microcavities. The thicknesses of BSFCz and BSTFCz layers were 39 and 32 nm, respectively. These thicknesses were carefully chosen to tune the lower polariton state at $k_{//} = 0$ close to the center wavelength of the DBR stopband to obtain a high cavity quality factor, and to ensure that the LPB have a good overlap with the emission spectrum for efficient radiative pumping of LP states

© 2021 The Authors. Laser & Photonics Reviews published by Wiley-VCH GmbH

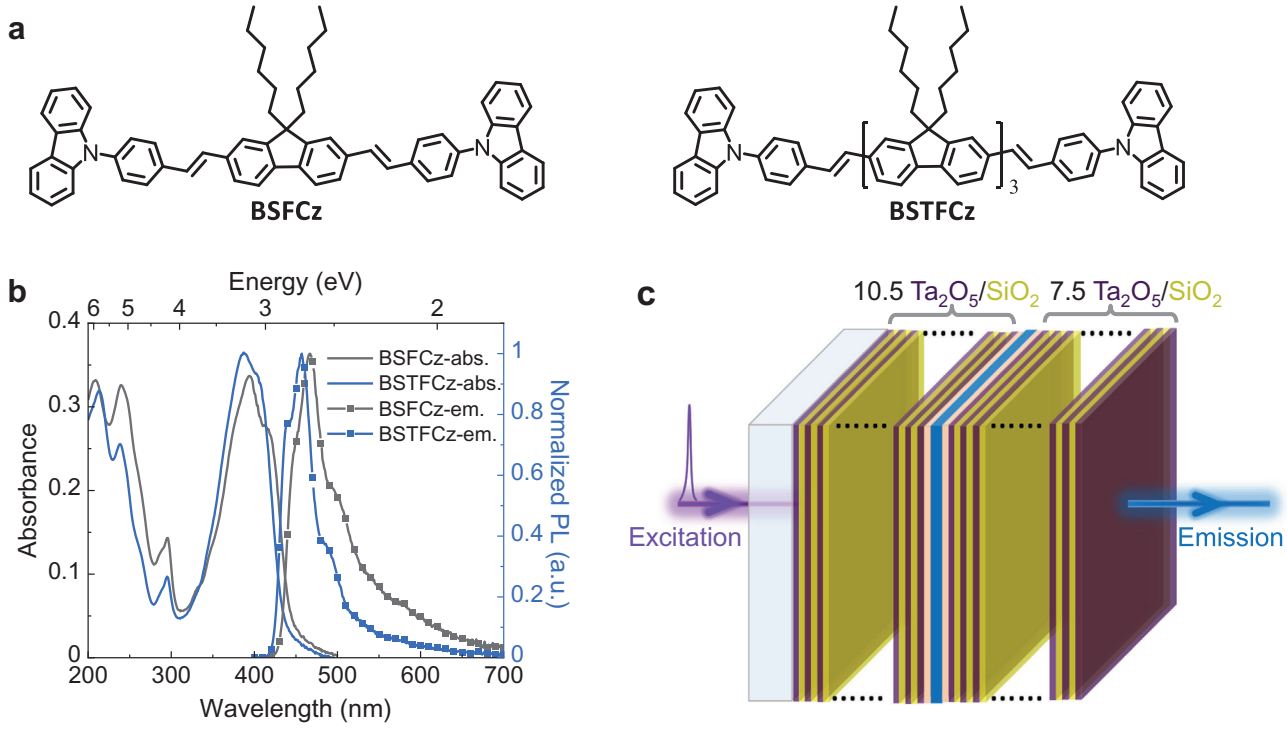

Figure 1. a) Molecular structure of BSFCz and BSTFCz. b) Absorption and emission spectra of neat BSFCz and BSTFCz films spin-coated on fused silica substrates. c) Schematic of DBR cavities. The layer at the centre in blue is the organic layer, while the two light orange layers are lithum fluoride (LiF).

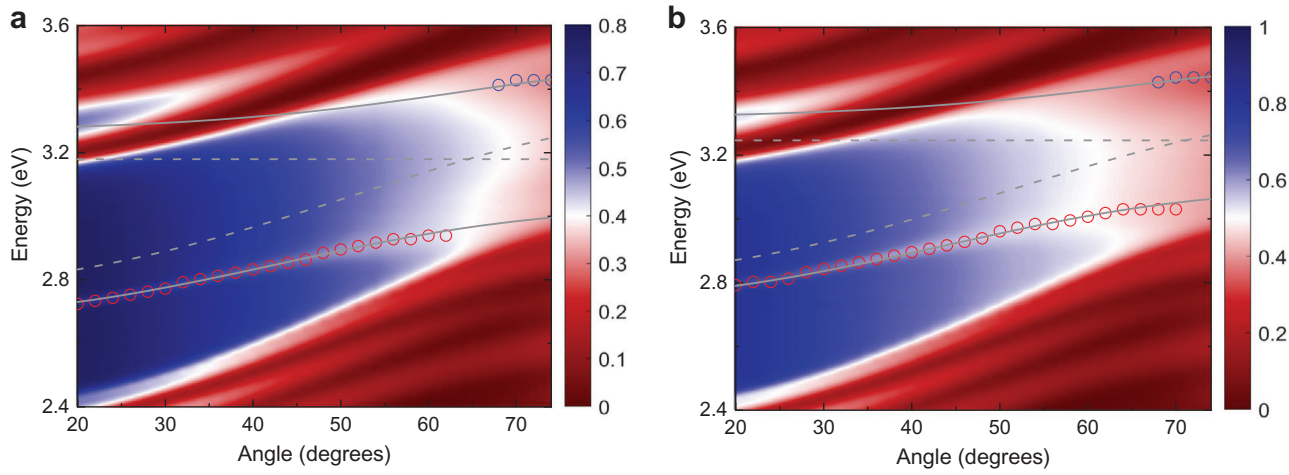

Figure 2. a,b) Color plots of p-polarized angle-resolved reflectivity for the BSFCz and BSTFCz cavities, respectively. Red and blue open circles are reflectivity minima at each angle extracted from measured reflectivity spectra. Gray solid lines trace coupled oscillator fit to reflectivity minima, gray dashed lines represent uncoupled exciton modes and cavity photon modes.

from the exciton reservoir. On either side of the emissive layer, a 50-nm-thick LiF was deposited to protect the active layer from plasma damage[13,30] during top DBR deposition as well as to ensure the active layers are located at the antinodes of cavity photon modes. The estimated quality factors of the microcavities were around 517 and 492 for the BSFCz and the BSTFCz cavities, respectively. The corresponding cavity photon lifetime values were 123 and 115 fs, respectively.

P-polarized white light reflectivity spectra were recorded as a function of incident angle from 20° to 74° as shown in **Figure 2**. The color map in Figure 2a plots the experimental data of the BSFCz cavity with a neat film thickness of 39 nm, the individual reflectivity spectrum at each angle is shown in Figure S1a in the Supporting Information. It can be clearly seen that two dispersive optical modes with different curvatures to the photonic DBR side bands undergo anticrossing around the wavelength of

© 2021 The Authors. Laser & Photonics Reviews published by Wiley-VCH GmbH

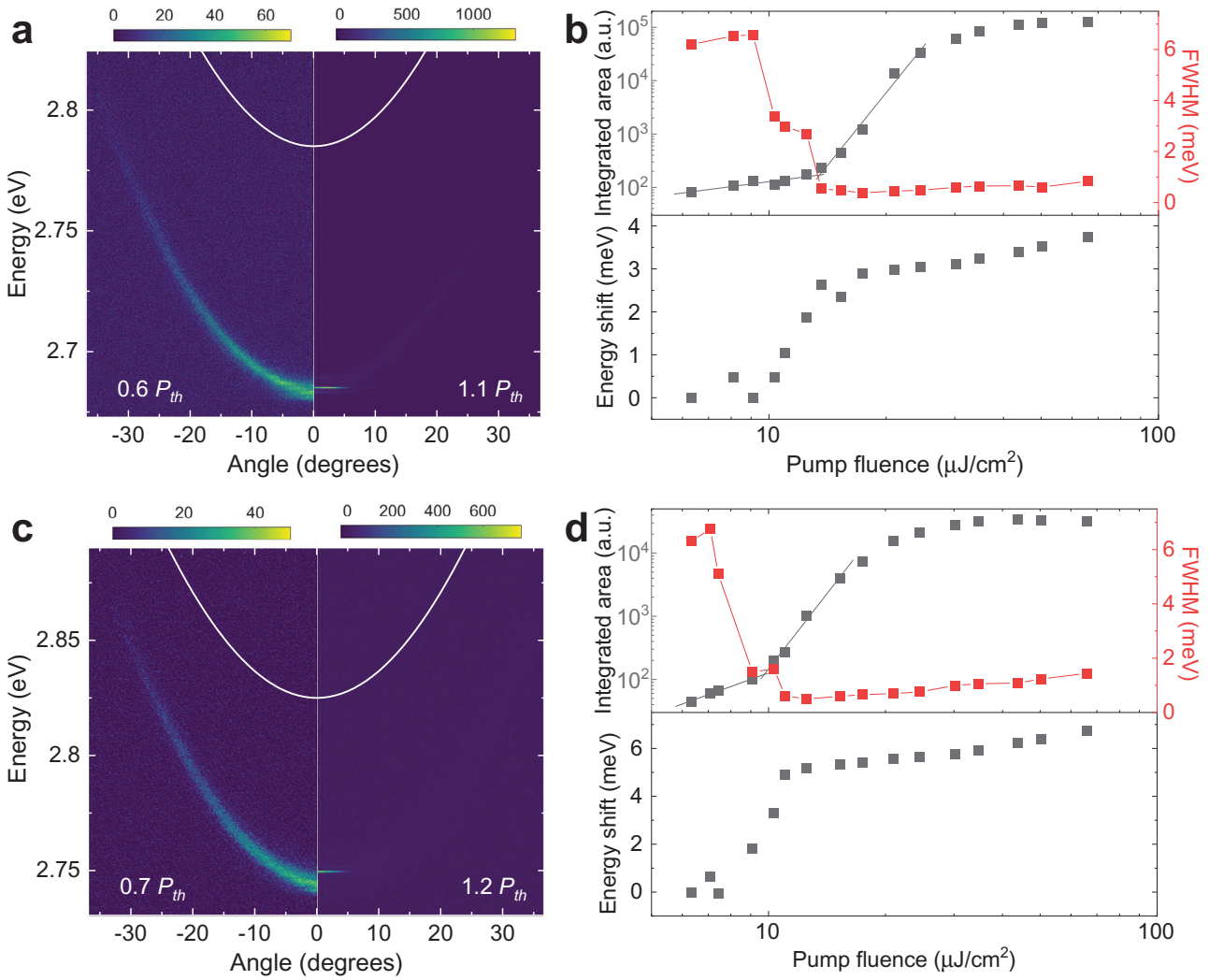

Figure 3. a,c) Vertically polarized angle-resolved emission below threshold (left half) and above threshold (right half) for a) the BSFCz cavity and c) the BSTFCz cavity. White curves are the cavity modes obtained from coupled oscillator models. b,d) Plot integrated area, FWHM, and energy shift of spectra at normal incidence as a function of pump fluence for the BSFCz cavity and the BSTFCz cavity, respectively. Black lines in the upper part of (b) and (d) are linear fits to integrated area values at different pump fluences.

the excitonic peak (3.18 eV) for the BSFCz cavity, indicating the cavity is in the strong exciton–photon coupling regime. The reflectivity minima of the BSFCz cavity were then extracted (open circles) and matched with a standard two-level coupled oscillator model. The fit results of the LPB and the UPB overlay as gray solid curves on the contour map in Figure 2a. From the coupled oscillator model, we also obtained the cavity photon mode (the parabolic dashed curve), a Rabi splitting energy of 430 meV and cavity detuning of −394 meV. The other fit parameters are listed in Table S1 in the Supporting Information. For the cavity detuning in the BSFCz cavity, the photon content at $k_{//} = 0$ of the LPB was calculated to be 84% as shown in Figure S2a in the Supporting Information.

The angle-resolved reflectivity spectra for a DBR cavity with 32-nm-thick BSTFCz neat film is shown as the contour map in Figure 2b, with a clear splitting between the two modes observed in the stopband. The anticrossing around the excitonic transition at 3.25 eV is an evident signature of strong coupling between BSTFCz excitons and the cavity mode. Fitting the LPB and UPB dispersion modes with a two-level coupled oscillator model as described in the Supporting Information yields a Rabi splitting of 384 meV, a cavity detuning of −421 meV, and a photon fraction of the LPB minimum of 87%. It is notable that the UPB is only visible at high angles in both cavities, which is attributed to the absorption from dark excitonic states.[31,32] S-polarized angle-resolved reflectivity of the two cavities was also measured and polarization splitting is observed in Figure S4 in the Supporting Information (Section S2, Supporting Information).

We subsequently characterized the emission properties of DBR cavities by exciting them non-resonantly at 343 nm using 200 fs pulses in a transmission geometry as shown in Figure 1c. **Figure 3**a presents vertically polarized angle-resolved PL of the BSFCz cavity at low (left panel) and high (right panel) pump fluences. At low pump fluence, the emission dispersion agrees well

© 2021 The Authors. Laser & Photonics Reviews published by Wiley-VCH GmbH

with that obtained from the angle-resolved reflectivity results in Figure 2a, indicating the BSFCz cavity is in the strong coupling regime. The uncoupled cavity mode shown as a white solid curve is detuned from the emission band. The intensity of emission reflects the photon fraction at the corresponding angles, which is consistent with the trend in Figure S2a in the Supporting Information. At high pump fluence, we observe an obvious collapse of the PL to the bottom of the branch, along with a narrowing of spectral linewidth and a blue-shift of the emission peak. Figure 3b plots the integrated PL intensity at $k_{//} = 0$ from 2.67 to 2.70 eV versus pump fluence. Individual spectra at each pump density at normal incidence are presented in Figure S5a in the Supporting Information. A super-linear increase of integrated intensity with increasing pump fluence is observed at an incident excitation density of 13.5 μJ cm^{-2}. Above the threshold pump fluence, the FWHM of spectra reduces from 6.2 to 0.4 meV. The cavity quality factor can be estimated from the FWHM at initial pump fluence to be 433 which is slightly lower than that obtained from calculation based on DBR reflectivity, indicating a relatively decent film morphology. We also observe a power-dependent blue-shift of the emission peak by up to 3.7 meV, which may be attributed to repulsive polariton–polariton, polariton-exciton interactions,[10,11,14,33] phase space filling and intermolecular energy migration.[34] These characteristics all provide evidence of polariton lasing in the BSFCz cavity.

The BSTFCz cavity was characterized in a similar way and the vertically polarized angle-resolved PL at low and high pump fluences are shown in Figure 3c. Similar hallmarks of polariton lasing are observed in the power-dependent emission data, including a macroscopic polariton occupation of the ground state above threshold, a nonlinear increase of integrated PL intensity from 2.73 to 2.77 eV, sudden decrease of spectral FWHM from 6.4 to 0.5 meV and a continuous blue-shift of 6.7 meV. The estimated cavity quality factor was 435. Detailed PL spectra at various excitation densities are shown in Figure S5b in the Supporting Information. From the top panel of Figure 3d, we can obtain a threshold of 9.7 μJ cm^{-2} from the evolution of integrated PL intensity at $k_{//} = 0$. This value is slightly lower than the threshold of the BSFCz cavity. Comparing with reported polariton lasing thresholds of organic semiconductors, which were summarized in a recent review by Keeling and Kéna-Cohen,[35] the threshold we obtain here is to our knowledge the lowest reported to date for planar organic microcavities, only half of the threshold of pentafluorene cavities.[13] As the BSFCz and BSTFCz cavities were pumped incoherently in the transparent sideband of DBRs, we also estimated the corresponding thresholds in terms of absorbed pump fluence, which are 3.3 and 2.2 μJ cm^{-2} for the two cavities, respectively, and are also the lowest reported to date by a large margin. As a result of this advance, we achieve for the first time, polariton lasers with pump threshold fluences as low as current state-of-the art organic cavity surface-emitting lasers with similar structures.[36–40] Our threshold is still slightly higher than of the very best organic distributed feedback (DFB) lasers because of the much longer interaction lengths with the gain material in such lateral structures[41] and the scope for precise control of feedback and output coupling (such as using substructured gratings[42]). The low polariton lasing thresholds in BSFCz and BSTFCz cavities are attributed to the simultaneous manifestation of strong absorption without severe concentration quenching leading to effective strong coupling, negligible exciton-exciton annihilation[26,43] of the two materials and increased radiative component of the LPB by negative detuning leading to the effective population of the LPB, and the relatively high quality factor of the two cavities. We anticipate further reducing the polariton lasing thresholds by optimizing the chemical structure of these laser dyes to increase neat film PLQYs, fine tuning the LPB to have a better overlap with the emission peak for more efficient radiative pumping of the LP states, and by increasing photonic confinement in an improved cavity configuration, such as 0D cavities, for higher quality factor.

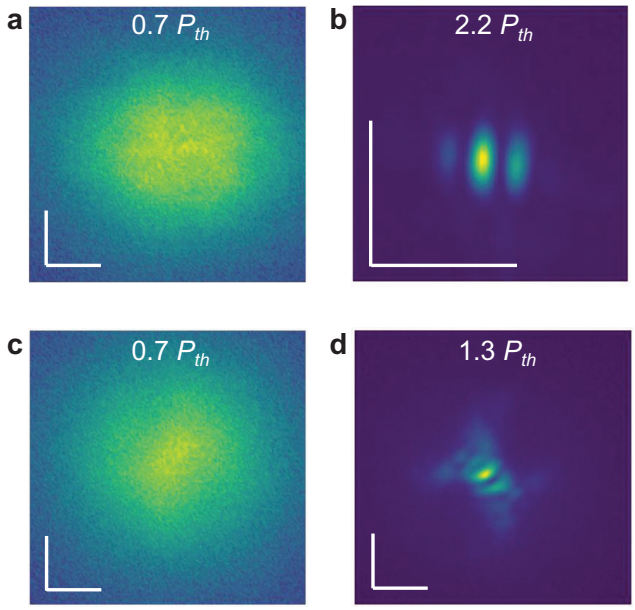

Figure 4. Interferograms of the BSFCz cavity a) below threshold (0.7 P_{th}, 9.1 μJ cm^{-2}) and b) above threshold (2.2 P_{th}, 30.2 μJ cm^{-2}). c,d) Interferograms of the BSTFCz cavity below threshold (0.7 P_{th}, 6.3 μJ cm^{-2}) and above threshold (1.3 P_{th}, 12.5 μJ cm^{-2}). All scale bars are 5 μm.

Another signature of polariton lasing is the blue-shift of emission peaks with increasing pump fluence, which we observe in both BSFCz and BSTFCz cavities. We note that the polariton blue-shift in the BSTFCz cavity is almost double that obtained in the BSFCz cavity, which may be attributed to the stronger effect from quenching of the Rabi splitting and the cavity mode renormalization in the BSTFCz cavity as anticipated from the vacuum Rabi splitting and the absorbed pump power at polariton lasing threshold. It is noticeable that the power-dependent blue-shifts plotted in Figure 3b,d exhibit a step-like increase at the polariton lasing threshold. This has been predicted and experimentally observed previously in organic microcavities and attributed to the interplay between the stimulated scattering to the polariton ground state and intermolecular energy transfer.[34]

A further characteristic of polariton lasing is long-range spatial coherence, which was measured by an adapted Michelson interferometer with one arm replaced by a retroreflector[44–46] in this work. **Figure 4**a shows the resulting interferogram of the BSFCz cavity below threshold at 0.7 P_{th} (9.1 μJ cm^{-2}) with no fringes. Individual real-space images from each arm are shown

© 2021 The Authors. Laser & Photonics Reviews published by Wiley-VCH GmbH

in Section S4 in the Supporting Information. Above threshold at 2.2 P_{th} (30.2 μJ cm^{-2}), the emission spot collapses to the one in Figure S6d (Supporting Information) with a diameter which is one eighth of the image in Figure S6a in the Supporting Information. The interferogram above threshold in Figure 4b has clear fringes over a range of 4 μm. The interferogram of the BSTFCz cavity below threshold at 0.7 P_{th} (6.3 μJ cm^{-2}) in Figure 4c shows no fringes as expected, discounting any possible effect from the excitation pulses. Above threshold at 1.3 P_{th} (12.5 μJ cm^{-2}), the emission spot condenses to several localized spots, which is consistent with the appearance of multi-peaks in the emission spectra above threshold (Figure S5b, Supporting Information). The resulting interferogram in Figure 4d is slightly disordered which may result from modulation instabilities in organic cavities,[46] leading to an intermediate fringe visibility of 45%, which is lower than that of the BSFCz cavity (87%). Nevertheless, it still shows macroscopic spatial coherence over 6 μm range. The line profile of interference fringes and corresponding fit to extract the fringe visibility are depicted in the Supporting Information.

3. Conclusion

We have demonstrated two new materials for room temperature polariton lasing. They are fluorene-based oligomers, BSFCz and BSTFCz, incorporating carbazole and dihexylfluorene units. The two molecules show excellent photophysical properties with solution processability to simplify the fabrication. Strong coupling between excitons and cavity photons was successfully observed in planar DBR cavities containing each of these two materials. Evidence for nonlinearity was presented in the angle-resolved PL spectra, including a nonlinear increase of PL intensity with increasing pump fluence, accompanied by a spectral linewidth narrowing of more than an order of magnitude and a step-like blue-shift at polariton lasing threshold, which is a signature of the interplay between the stimulated exciton relaxation and intermolecular energy transfer. Our results show that narrow excitonic linewidth is not essential for realizing polariton lasing if Rabi splitting is large enough. The respective incident optically pumped polariton lasing thresholds for the BSFCz and the BSTFCz cavities were 13.5 and 9.7 μJ cm^{-2}, corresponding to absorbed thresholds of 3.3 and 2.2 μJ cm^{-2}, which are the lowest reported thresholds for organic microcavities and are a significant advance as they bring polariton laser thresholds down to the levels of the best organic photon lasers with planar cavity or DFB configurations. The results indicate that material properties, including high absorption coefficient, high radiative decay rates, and negligible exciton–exciton annihilation, play key roles in achieving very low thresholds. A low lasing threshold is very important for practical applications of such coherent light emitters as it reduces the demands on the pump source, and is a necessary step for future realization of electrically injected polariton lasers.

4. Experimental Section

Fabrication: The synthetic methods of BSFCz and BSTFCz were reported elsewhere.[26,27] For photophysical characterization, including absorption, PL, PLQY, and optical constants, BSFCz and BSTFCz were dissolved readily in chlorobenzene at a concentration of 8 mg mL^{-1}. Neat films with thickness of 30 nm were obtained by spin-coating at a speed of 3000 rpm from solution on precleaned fused silica substrates.

For the fabrication of microcavities, 10.5 pairs of Ta_2O_5/SiO_2 with respective thicknesses of 49.7 and 74 nm were deposited on fused silica substrates by radio-frequency magnetron sputtering as the bottom DBRs, followed by thermal evaporation of 50-nm-thick LiF as a spacer layer. The active layer was then spin-coated from BSFCz or BSTFCz solution at a concentration of 15 mg mL^{-1}. A further layer of 50-nm LiF was then deposited to protect the active layer from plasma damage[13,46] during top DBR deposition as well as to ensure the active layers are located at the antinodes of cavity photon modes. The microcavities were completed by sputtering 7.5 pairs of Ta_2O_5/SiO_2 as the top DBRs. The sample preparation process, including that of both bare films and cavities, was carried out in a nitrogen filled glovebox.

Characterization: Absorption and PL spectra were measured using a Cary 300 UV-Visible spectrophotometer and an Edinburgh Instruments FLS980 PL spectrometer, respectively. PLQY measurements of neat films were performed in an integrating sphere[47] in a Hamamatsu Photonics C9920-02 absolute PLQY spectrometer using a Xenon lamp as the light source. The optical constants and film thickness of bare films were measured by a J.A. Woollam M-2000DI spectroscopic ellipsometer.

Polarized angle-resolved reflectance spectroscopy of microcavities was conducted using the same ellipsometer with a dual deuterium and quartz tungsten halogen light source to provide a wide spectral range from 245 to 1690 nm. An automated sample platform and detection arms enabled collection of reflectivity spectra at incidence angles from 20° to 74° with an interval of 2°. Angle-resolved PL measurements were undertaken using Fourier imaging spectroscopy. A femtosecond pulsed, vertically polarized pump laser of wavelength 343 nm excited microcavities at around normal incidence through the sample substrates. The UV pump beam was the third harmonic from a Pharos laser system (Light Conversion) with a pulse duration of 200 fs and a repetition rate of 5 kHz. The diameter of the Gaussian pump beam was measured to be around 30 μm. Emission from the microcavities was collected by a microscope objective (Nikon, S Plan Fluor ELWD 40X) with a numerical aperture of 0.6 and directed into an Andor Shamrock SR500i imaging spectrometer. A sheet polarizer was placed between two Fourier transform lenses to distinguish vertically and horizontally polarized emission from the cavities. To block residual signal from the pump beam, a 400 nm long pass filter was mounted in front of the slit of the spectrometer. PL spectra were recorded in wavelength and angle by an 1800 grooves per mm grating, providing a spectral resolution of 0.012 nm.

For the spatial coherence study, a Michelson interferometer with one arm replaced by a broadband hollow retroreflector was used to obtain interferograms. Collimated emission light from the microcavities was split by a nonpolarizing cube beam splitter in the interferometer. Spatially resolved images were recorded by the CCD camera with the spectrometer slit fully open and grating aligned for zero order reflection. The spatial coherence measurements and angle-resolved spectroscopy studies were all performed in ambient conditions.

Supporting Information

Supporting Information is available from the Wiley Online Library or from the author.

Acknowledgements

The authors are grateful to the Australian Research Council (ARC DP160100700 and DP200103036), Australian Department of Industry, Innovation and Science (AISRF53765), the UK Engineering and Physical Sciences Research Council (Grants EP/M025330/1 and EP/L017008/1), China Scholarship Council and the Rank Prize Funds for financial support.

© 2021 The Authors. Laser & Photonics Reviews published by Wiley-VCH GmbH

Conflict of Interest

The authors declare no conflict of interest.

Data Availability Statement

The data that support the findings of this study are openly available in University of St Andrews Research Portal at https://doi.org/10.17630/bdb15177-5309-4f34-9c31-1882fbaeb83f.[48]

Keywords

excitons, microcavities, organic semiconductors, strong light–matter coupling

Received: January 20, 2021
Revised: March 30, 2021
Published online:

[1] S. I. Pekar, *J. Exp. Theor. Phys.* **1958**, *6*, 4.
[2] J. J. Hopfield, *Phys. Rev.* **1958**, *112*, 1555.
[3] R. J. Holmes, S. R. Forrest, *Org. Electron.* **2007**, *8*, 77.
[4] A. Kavokin, J. J. Baumberg, G. Malpuech, F. P. Laussy, *Microcavities*, Oxford University Press, Oxford, UK **2011**.
[5] A. Das, J. Heo, M. Jankowski, W. Guo, L. Zhang, H. Deng, P. Bhattacharya, *Phys. Rev. Lett.* **2011**, *107*, 066405.
[6] P. Bhattacharya, T. Frost, S. Deshpande, M. Z. Baten, A. Hazari, A. Das, *Phys. Rev. Lett.* **2014**, *112*, 236802.
[7] C. P. Dietrich, A. Steude, L. Tropf, M. Schubert, N. M. Kronenberg, K. Ostermann, S. Höfling, M. C. Gather, *Sci. Adv.* **2016**, *2*, e1600666.
[8] D. G. Lidzey, D. D. C. Bradley, M. S. Skolnick, T. Virgili, S. Walker, D. M. Whittaker, *Nature* **1998**, *395*, 53.
[9] S. Kéna-Cohen, S. R. Forrest, *Nat. Photonics* **2010**, *4*, 371.
[10] K. S. Daskalakis, S. A. Maier, R. Murray, S. Kéna-Cohen, *Nat. Mater.* **2014**, *13*, 271.
[11] T. Cookson, K. Georgiou, A. Zasedatelev, R. T. Grant, T. Virgili, M. Cavazzini, F. Galeotti, C. Clark, N. G. Berloff, D. G. Lidzey, P. G. Lagoudakis, *Adv. Opt. Mater.* **2017**, *5*, 1700203.
[12] D. Sannikov, T. Yagafarov, K. Georgiou, A. Zasedatelev, A. Baranikov, L. Gai, Z. Shen, D. Lidzey, P. Lagoudakis, *Adv. Opt. Mater.* **2019**, *7*, 1900163.
[13] S. K. Rajendran, M. Wei, H. Ohadi, A. Ruseckas, G. A. Turnbull, I. D. W. Samuel, *Adv. Opt. Mater.* **2019**, *7*, 1801791.
[14] J. D. Plumhof, T. Stöferle, L. Mai, U. Scherf, R. Mahrt, *Nat. Mater.* **2014**, *13*, 247.
[15] M. Wei, S. K. Rajendran, H. Ohadi, L. Tropf, M. C. Gather, G. A. Turnbull, I. D. W. Samuel, *Optica* **2019**, *6*, 1124.
[16] S. Betzold, M. Dusel, O. Kyriienko, C. P. Dietrich, S. Klembt, J. Ohmer, U. Fischer, I. A. Shelykh, C. Schneider, S. Höfling, *ACS Photonics* **2020**, *7*, 384.
[17] A. Genco, A. Ridolfo, S. Savasta, S. Patanè, G. Gigli, M. Mazzeo, *Adv. Opt. Mater.* **2018**, *6*, 1800364.
[18] A. K. Bansal, A. Ruseckas, P. E. Shaw, I. D. W. Samuel, *J. Phys. Chem. C* **2010**, *114*, 17864.
[19] M. Grell, D. D. C. Bradley, G. Ungar, J. Hill, K. S. Whitehead, *Macromolecules* **1999**, *32*, 5810.
[20] A. J. Cadby, P. A. Lane, H. Mellor, S. J. Martin, M. Grell, C. Giebeler, D. D. C. Bradley, M. Wohlgenannt, C. An, Z. V. Vardeny, *Phys. Rev. B* **2000**, *62*, 15604.
[21] P. E. Shaw, A. Ruseckas, J. Peet, G. C. Bazan, I. D. W. Samuel, *Adv. Funct. Mater.* **2010**, *20*, 155.
[22] T. Aimono, Y. Kawamura, K. Goushi, H. Yamamoto, H. Sasabe, C. Adachi, *Appl. Phys. Lett.* **2005**, *86*, 071110.
[23] A. S. D. Sandanayaka, K. Yoshida, M. Inoue, C. Qin, K. Goushi, J. C. Ribierre, T. Matsushima, C. Adachi, *Adv. Opt. Mater.* **2016**, *4*, 834.
[24] A. S. D. Sandanayaka, T. Matsushima, F. Bencheikh, K. Yoshida, M. Inoue, T. Fujihara, K. Goushi, J. C. Ribierre, C. Adachi, *Sci. Adv.* **2017**, *3*, e1602570.
[25] M. Mamada, T. Fukunaga, F. Bencheikh, A. S. D. Sandanayaka, C. Adachi, *Adv. Funct. Mater.* **2018**, *28*, 1802310.
[26] V. T. N. Mai, A. Shukla, A. M. C. Senevirathne, I. Allison, H. Lim, R. J. Lepage, S. K. M. Mcgregor, M. Wood, T. Matsushima, E. G. Moore, E. H. Krenske, A. S. D. Sandanayaka, C. Adachi, E. B. Namdas, S. Lo, *Adv. Opt. Mater.* **2020**, *8*, 2001234.
[27] A. Shukla, V. T. N. Mai, A. M. C. Senevirathne, I. Allison, S. K. M. Mcgregor, R. J. Lepage, M. Wood, T. Matsushima, E. G. Moore, E. H. Krenske, A. S. D. Sandanayaka, C. Adachi, E. B. Namdas, S. Lo, *Adv. Opt. Mater.* **2020**, *8*, 2000784.
[28] S. Schumacher, A. Ruseckas, N. A. Montgomery, P. J. Skabara, A. L. Kanibolotsky, M. J. Paterson, I. Galbraith, G. A. Turnbull, I. D. W. Samuel, *J. Chem. Phys.* **2009**, *131*, 154906.
[29] J. Shi, Y. Wu, S. Sun, B. Tong, J. Zhi, Y. Dong, *J. Polym. Sci., Part A: Polym. Chem.* **2013**, *51*, 229.
[30] L. S. Hung, L. S. Liao, C. S. Lee, S. T. Lee, *J. Appl. Phys.* **1999**, *86*, 4607.
[31] R. Houdré, R. P. Stanley, M. Ilegems, *Phys. Rev. A* **1996**, *53*, 2711.
[32] J. A. Cwik, P. Kirton, S. De Liberato, J. Keeling, *Phys. Rev. A* **2016**, *93*, 1.
[33] M. Vladimirova, S. Cronenberger, D. Scalbert, K. V. Kavokin, A. Miard, A. Lemaître, J. Bloch, D. Solnyshkov, G. Malpuech, A. V. Kavokin, *Phys. Rev. B* **2010**, *82*, 075301.
[34] T. Yagafarov, D. Sannikov, A. Zasedatelev, K. Georgiou, A. Baranikov, O. Kyriienko, I. Shelykh, L. Gai, Z. Shen, D. Lidzey, P. Lagoudakis, *Commun. Phys.* **2020**, *3*, 1.
[35] J. Keeling, S. Kéna-Cohen, *Annu. Rev. Phys. Chem.* **2020**, *71*, 435.
[36] L. Persano, P. Del Carro, E. Mele, R. Cingolani, D. Pisignano, M. Zavelani-Rossi, S. Longhi, G. Lanzani, *Appl. Phys. Lett.* **2006**, *88*, 121110.
[37] T. Virgili, D. G. Lidzey, M. Grell, D. D. C. Bradley, S. A. Stagira, M. A. Zavelani-Rossi, S. A. De Silvestri, *Appl. Phys. Lett.* **2002**, *80*, 4088.
[38] G. Canazza, F. Scotognella, G. Lanzani, S. De Silvestri, M. Zavelani-Rossi, D. Comoretto, *Laser Phys. Lett.* **2014**, *11*, 035804.
[39] M. Theander, T. Granlund, D. M. Johanson, A. Ruseckas, V. Sundström, *Adv. Mater.* **2001**, *13*, 323.
[40] Y. Hu, F. Bencheikh, S. Chénais, S. Forget, X. Liu, C. Adachi, *Appl. Phys. Lett.* **2020**, *117*, 153301.
[41] C. Karnutsch, C. Pflumm, G. Heliotis, J. C. Demello, D. D. C. Bradley, J. Wang, T. Weimann, V. Haug, C. Gärtner, U. Lemmer, *Appl. Phys. Lett.* **2007**, *90*, 131104.
[42] E. R. Martins, Y. Wang, A. L. Kanibolotsky, P. J. Skabara, G. A. Turnbull, I. D. W. Samuel, *Adv. Opt. Mater.* **2013**, *1*, 563.
[43] G. M. Akselrod, Y. R. Tischler, E. R. Young, D. G. Nocera, V. Bulovic, *Phys. Rev. B* **2010**, *82*, 113106.
[44] J. Kasprzak, M. Richard, S. Kundermann, A. Baas, P. Jeambrun, J. M. J. Keeling, F. M. Marchetti, M. H. Szymánska, R. André, J. L. Staehli, V. Savona, P. B. Littlewood, B. Deveaud, L. S. Dang, *Nature* **2006**, *443*, 409.
[45] G. Roumpos, M. Lohse, W. H. Nitsche, J. Keeling, M. H. Szymańska, P. B. Littlewood, A. Löffler, S. Höfling, L. Worschechh, A. Forchel, Y. Yamamoto, *Proc. Natl. Acad. Sci. USA* **2012**, *109*, 6467.

© 2021 The Authors. Laser & Photonics Reviews published by Wiley-VCH GmbH

[46] K. S. Daskalakis, S. A. Maier, S. Kéna-Cohen, *Phys. Rev. Lett.* **2015**, *115*, 035301.
[47] N. C. Greenham, I. D. W. Samuel, G. R. Hayes, R. T. Phillips, Y. A. R. R. Kessener, S. C. Moratti, A. B. Holmes, R. H. Friend, *Chem. Phys. Lett.* **1995**, *241*, 89.
[48] M. Wei, A. Ruseckas, V. T. N. Mai, A. Shukla, I. Allison, S.-C. Lo, E. B. Namdas, G. A. Turnbull, I. D. W. Samuel, **2021**, Low-Threshold Room Temperature Polariton Lasing from Fluorene-Based Oligomers (dataset). Dataset. University of St Andrews Research Portal. [https://doi.org/10.17630/bdb15177-5309-4f34-9c31-1882fbaeb83f]

© 2021 The Authors. Laser & Photonics Reviews published by Wiley-VCH GmbH